Supplementary Information for

Tip Optofluidic Immunoassay: Evaluating COVID-19 Antibody Protection with 1μL Fingertip Blood

Xiaotian Tan[1,2,*,#], Yujuan Chai[3,*,#], Ruihan Li[1,2,#], Binmao Zhang[3,1,#], Hao Li[4,1#], Jie Zhang[5], Tianen Zhu[6], Weishu Wu[7], Lixiang An[4], Shi Hu[1,2,8], Bin Yang[5], Li Wang[5], Zhenqiu Cao[9], Hongjiu Zhang[9], Peng Wang[10], Lingling Yu[10], Shan Yin[10], Xingyu Li[10], Fei Shao[10], Jianheng Huang[3,1], Jinze Li[1], Fan Yang[2,11], Chao Zhao[1,2], Jiajia Guo[1,2], Lin Zeng[1,2], Dong Liang[1,2], Zhengting Zou[9], Hairong Zheng[1,2]*, Xudong Fan[7]*, Liangzhi Xie[5,12,13]*, Yunlong Cao[10,14]*, and Hui Yang[1,2]*

1. Institute of Biomedical and Health Engineering, Shenzhen Institute of Advanced Science, Chinese Academy of Science, Shenzhen 518055, China.
2. The Key Laboratory of Biomedical Imaging Science and System, Chinese Academy of Sciences, Shenzhen 518055, China.
3. Department of Biomedical Engineering, Shenzhen University Medical School, Shenzhen University, Shenzhen 518060, China.
4. National Innovation Center for Advanced Medical Devices, Shenzhen 518110, China.
5. Beijing Key Laboratory of Monoclonal Antibody Research and Development, Sino Biological Inc., Beijing 100176, China.
6. Emergency Department, Shenzhen University General Hospital, Shenzhen University, Shenzhen 518060, China.
7. Department of Biomedical Engineering, University of Michigan, MI 48109, USA.
8. University of Chinese Academy of Science, Beijing 101408, China.
9. Institute of Zoology, Chinese Academy of Science, Beijing 100101, China.
10. Changping Laboratory, Beijing 102206, China.
11. Institute of Biomedicine and Biotechnology, Shenzhen Institute of Advanced Science,

Chinese Academy of Science, Shenzhen 518055, China.

12. Beijing Engineering Research Center of Protein and Antibody, Sinocelltech Ltd., Beijing, China.
13. Beijing Engineering Research Center of Protein and Antibody, Sinocelltech Ltd., Beijing, China.
14. BIOPIC, Peking University, Beijing 100871, China.

# Equally contributed

* Corresponding authors

xt.tan@siat.ac.cn; chaiyj@szu.edu.cn; hr.zheng@siat.ac.cn; xsfan@umich.edu; LX@sinocelltech.com; yunlongcao@pku.edu.cn; hui.yang@siat.ac.cn;

Materials and Methods:

Portable Tip Optofluidic Immunoassay System (TOI)

The TOI system is composed mainly of two sections: (1) microfluidic immuno-reactors and (2) portable chemiluminescent imaging station. The immuno-reactors are used as disposable structures for conducting immunosorbent assays with fingertip blood samples; the chemiluminescent imaging station is designed to quantitatively measure the chemiluminescent signal intensities of the immuno-reactors (Fig. 1). Detailed information for the two sections can be found below:

Microfluidic Immuno-reactors

The microfluidic immuno-reactors were fabricated through injection molding with high-protein affinity polystyrene, with technical support from Beijing 4.0 Industrial Technology Co., Ltd. The microfluidic immuno-reactors are composed of three units: sensing unit, intersection, and adapting unit. The inner diameter of the microfluidic immuno-reactors is 0.9 mm. As presented in Figure S1A-D, the industrial-grade mass microfabrication of the reactors could achieve a qualified yield of over 99.9 % for each batch of product (~10000), indicating a high reliability. To perform an immunoassay, the microfluidic immuno-reactors will be connected to standard 20-200 μL pipette tips for liquid handling. No chemical surface treatment is needed before each immunoassay. The evaluation of protein immobilization kinetics for the microfluidic immuno-reactors is shown in Figure S2A. For common proteins such as IgG, physical adsorption generally saturates after 20-40 minutes, which is significantly faster than conventional immunoassay reactors like 96-well plates.

Portable Chemiluminescent Imaging Station

To simplify the platform structure to the greatest extent, the chemiluminescence imaging method was chosen for immunoassay signal measurement. The portable chemiluminescent imaging station (PCIS) was designed and assembled in-house. As presented in Figure S3, the PCIS includes a shading cover (stainless steel), a pipette

holder (also works as the immuno-reactors), and a CMOS camera. The total weight of the signal measurement box is about 3 kg, which is easy to carry with one hand.

The intensity of the chemiluminescence signal is generally very weak. Thus, the protection against environmental light interference is a key factor in the design of the signal measurement box. Light-protection structures are placed in all corners and connecting sections. To perform accurate and quantitative measurements of the chemiluminescent system, we used a highly sensitive monochromic CMOS camera QHY533M (from QHYCCD) along with a Fujinon wide-angle micro-distance lens to collect long-exposure chemiluminescent images. The camera is placed 12.5 cm in front of the pipette holder. The pipette holder (fabricated through 3D printing) is designed to stabilize the multi-channel pipette and the attached immuno-reactors attached. Vertical walls are built between the microfluidic immuno-reactors to prevent inter-channel crosstalk.

The optical quantification performance of the QHY533M camera can be found in Figure S2B. The minimum detectable optical signal intensity was 1.0, and the linear dynamic range was about 60,000 (at gain = 70), covering 4.5-5 orders of magnitude in optical signal intensity.

Chemiluminescent Signal Quantification

After the final reaction step, the multichannel pipette with the microfluidic immuno-rectors will be placed in the PCIS for chemiluminescence intensity measurement. The baseline is calculated as the average blank signal intensity for the device. Based on our optimization results, 6 s exposure time is suitable for most of the chemiluminescence intensity quantification applications.

Biomolecular and Chemical Reagents

All fundamental chemical reagents, including 10 × PBS buffer, pH=7.4 (AM9624), wash buffer (0.05% Tween-20 in PBS), and luminol chemiluminescence substrate (SuperSignal™ ELISA Femto Substrate, 37075) were purchased from Thermo Fisher. All protein buffers, including 10% Blocker™ BSA (in PBS, 37525), 1% casein (in PBS,

poly-HRP dilution buffer, N500), and SuperBlock^{TM} buffer (in PBS, 37515) were also purchased from Thermo Fisher.

For biomolecular reagents, broad-spectrum SARS-CoV-2 antibodies SA55 and SA58 were developed and provided by Dr. Yunlong Cao from Peking University. Recombinant SARS-CoV-2 RBDs (40592-V08H for WT, 40592-V08H136 for XBB.1.16), recombinant SARS-CoV-2 spike ectodomain (S-ECD) homotrimers (40589-V08H8 for WT, 40589-V08H48 for XBB.1.16) and recombinant SARS-CoV-2 antibody D006 (40589-D006) were all produced and provided by Sino Biological. The monoclonal anti-human-IgG antibody (HRP conjugated) was also developed and provided by Sino Biological. The streptavidin labeled poly-HRP (SA poly-HRP) was purchased from Thermo Fisher (21140).

Assay Protocol with Recombinant SARS-Cov-2 Specific Human IgG

For SARS-CoV-2 IgG binding assays with recombinant antibodies, antigenic proteins (RBDs or S-ECD homotrimers) were first immobilized on the inner surface of the immuno-reactors. The working solution of protein was in 1 × PBS (pH = 7.4) at 10 μg/mL. Two consecutive blocking steps (3% BSA in PBS + SuperBlock^{TM} buffer) were used to reduce the noise level. The immuno-reactors were rinsed once after each incubation step. A graphical illustration of the assay protocol can be found in Figure S4.

For concept demonstration, standard antibody solutions at different concentrations were tested with TOI. Three recombinant SARS-CoV-2 IgGs (SA55[33, 34], SA58[35, 36], D006[37]) were evaluated in this assay (Fig. 2). The working solutions of the antibodies were first prepared by diluting the stock solution with 1% casein in PBS. Fourfold serial-diluted antibody solutions were drawn into the reactors to react with protein immobilized on the reactor's inner surface and left at room temperature to react. The incubation time for the antibody solutions was 8 minutes. Subsequently, HRP-conjugated detection antibody solution (6000 × diluted with 1% casein in PBS, ~170 ng/mL) was applied to the immuno-reactors. The incubation time for the detection antibody solutions was three minutes. Finally, a chemiluminescent substrate was

introduced to the immuno-reactors after rinsing in triplicate. The optimization of the blocking and dilution buffer can be found in Figure S5&S6. Using 1% casein in PBS for both immuno-reactor blocking and sample/reagent dilution significantly reduced the background noise level to a nearly non-detectable level.

Human Sample Collection

The research protocol and the collection of human blood samples, including fingertip blood, fingertip serum, venous blood, and venous serum were approved by the Institutional Review Broad (IRB) of Shenzhen Institute of Advanced Science, Chinese Academy of Science (SIAT-IRB-230715-H0667). With the informed consent of all participants, venous blood samples were collected by trained experts using vacuum blood collection tubes, while fingertip blood samples were collected with pain-free fingertip blood pens that were designed for routine blood glucose monitoring. Fingertip serum samples were generated by centrifuging 30 μL of fingertip blood for three minutes at 3000 g. For all volunteers, the fingertip blood was diluted 25 × using 1% casein in PBS, followed by a quick spin for the removal of the pellet (i.e. red blood cells) before storage at -20℃ (Fig. S7) All other types of samples were also diluted with 1% casein in PBS before applying to TOI. The first round of sample collection was conducted in September 2023, involving 113 individuals. The second round of sample collection was conducted in March 2024, involving 22 individuals from the first round of sample collection. The negative control sample was obtained from one of our previous clinical studies, which was approved by the IRB of the Second Affiliated Hospital of Chongqing Medical University (No. 2018 (100))[32]. The blood sample was collected before the COVID-19 outbreak and stored at -20 ℃ without freeze and thaw ever since. The informed consent of this study was obtained through re-contact of the healthy blood donor of the sample.

Binding IgG titration curves for different sample types

The binding IgG titration assays for different sample types were conducted with

blood samples of 6 volunteers using a protocol that was generally consistent with the proof-of-concept experiments. To generate a six-point titration curve for SARS-Cov-2 specific IgG, whole blood/serum was prepared and stored as described in the previous section. Various final concentrations were prepared by further diluting the stock solution with 1% casein. The final dilution factors of the samples were 50, 250, 1250, 6250, 31250, and 156250 fold. A negative control serum collected before the COVID-19 outbreak (without SARS or MERS infection history) was also applied and served as a baseline for the TOI (Fig. 3).

Binding IgG Quantification and Binding Kinetic Evaluation of the Blood Samples

In the SARS-CoV-2 binding IgG quantification study, 1 μL fingertip blood was evaluated for 135 volunteer samples (Fig. 4). All volunteers were numbered for de-identification during testing. However, their background information including age, gender, COVID-19 vaccination records, and infection history were recorded upon participation and unblinded upon data analysis. To evaluate the SARS-CoV-2-specific IgG binding capacity of volunteers quantitatively, the results of this assay were converted to the equivalent concentrations of a therapeutic antibody, SA55 (ref). The effective SA55 concentration was measured with a three-point calibration curve established with standard SA55 solutions of 100, 20, and 4 ng/mL, and served as the internal reference in each assay. Among all 113 participants invited in the first round of sampling in September 2023, 22 were re-sampled and examined again in March 2024. All of them experienced flu-like syndrome during the six months, with several confirmed to have SARS-CoV-2 infection.

The IgG binding kinetics assays for blood samples were also carried out using a similar protocol aforementioned (Fig. S4B). To evaluate the binding kinetics of the antibodies, the sample incubation times were set to 2, 4, and 8 minutes (Fig. 5).

Design and Construction of the Engineered Proteins used in RIVIA 2.0

For RIVIA 2.0, a recombinant human ACE2 (hACE2) was designed, expressed, and

provided by Sino Biological Inc., containing an active hACE2 ECD, a human IgG-Fc domain, and a spacer in between (hACE2-hFc, 10108-H02H). The IgG-Fc domain was primarily used in protein purification but also serves as the anchor for immobilization on TOI microfluidic immuno-reactors. The hACE2-hFc serves as the mock receptor for SARS-CoV-2 spike proteins in the RIVIA assays (Fig.S8 & Fig. 6).

Additionally, a specially designed S-ECD of WT and XBB.1.16 strains were also expressed and purified by Sino Biological Inc. Each engineered monomer contains an S-ECD, a T4 trimerization domain, an Avi-tag, and a biotin on the N-terminal. The Avi-tag biotinylation was designed to provide orientation-specific labeling that can maximize the binding and signaling efficiency. Due to the presence of the T4 trimerization domain, the homotrimer of the engineered S-ECD will form automatically. AlphaFold3 simulations for these two proteins can be found in Figure S8, and an illustrational comparison between the biotinylated S-ECD trimers used in our original RIVIA and RIVIA 2.0 can be found in Figure S9.

Optimization of RIVIA 2.0

For the RIVIA 2.0 assay, the recombinant human ACE2 was first immobilized on the inner surface of the TOI immuno-reactors through one-hour physical adsorption at 15 μg/mL. After the two consecutive blocking steps, the sample and S-ECD mixture solution were drawn into the TOI immuno-reactors. The final concentration of the engineered AVI-tag biotinylated S-ECD homotrimer was 10 ng/mL. This concentration was chosen to produce a stable and strong chemiluminescence signal under the same conditions in the absence of antibodies or nanobodies. The optimization of S-ECD homotrimer concentration can be found in Figure S10. For chemiluminescent signal measurement, 3000 × diluted SA poly-HRP solution was used for the visualization of the biotinylated S-ECD attached to the reactor surface.

Performance Evaluation of the RIVIA 2.0.

To construct the calibration curves of RIVIA 2.0, various concentrations of SA55,

SA58, and D006 were prepared through serial dilutions. The fingertip blood samples collected from volunteers were tested at 50 × dilution and incubated for 10 minutes in the immuno-reactors. For each set of assays (12 reactors), one of the immuno-reactors was used as the positive control (1 μg/mL SA55), and two were used as the negative controls (1% casein in PBS). The CVs of RIVIA 2.0 were also obtained with 6 repeated tests of 1 μg/mL SA55 and SA58 as mock samples.

Conventional Pseudovirus Neutralization Test (pVNT)

To generate the pseudovirus, the spike (S) protein gene of the SARS-CoV-2 variant was codon optimized and inserted into the pcDNA3.1 vector. The vector containing the S protein gene was co-transfected with the G*ΔG-VSV virus (Kerafast, EH1020-PM) into 293T cells (ATCC, CRL-3216). After cell culturing, the supernatant was collected by centrifugation, filtered, and aliquoted for storage.

In a 96-well cell culture plate, the serum to be tested was diluted in a gradient using DMEM medium (Hyclone, SH30243.01). The pseudovirus was then added, and the mixture was incubated at 37°C for 1 hour. Huh-7 cells (Japanese Collection of Research Bioresources (JCRB), 0403) were digested into a single-cell suspension, added to the wells, and incubated at 37°C with 5% CO2 for approximately 24 hours. Half of the supernatant was then discarded, and Bright-Lite Luciferase Assay Substrate (lyophilized) mixed with Bright-Lite Luciferase Assay Buffer (Vazyme, DD1209-03-AB) was added. The plate was then kept in the dark to allow the reaction to proceed. The cell lysate was transferred to a white 96-well detection plate, and luminescence intensity was measured using a microplate spectrophotometer. Dose-response curves were fitted using a four-parameter logistic regression model to calculate the half-maximal inhibitory concentration (IC50).

Principal Component Analysis (PCA) and Phylogenetic Inference of RBDs

The pre-trained protein language model ESM-MSA-1b[1,2] was downloaded from https://dl.fbaipublicfiles.com/fair-esm/models/esm_msa1b_t12_100M_UR50S.pt

shown on the ESM GitHub page (https://github.com/facebookresearch/esm). Intact S protein sequences were aligned by MAFFT v7.505[3] using the linsi algorithm. Selected SARS-CoV-2 RBD domains (SARS, WT, Alpha, Beta, Gamma, Delta, D614G, Omicron BA1, BA2, BA3, BA.4/5, XBB.1.5., XBB.1, EG.5, JN.1, and BA2.86) were extracted from the alignment, and each sequence with gaps was encoded by ESM alphabet. Start token '<cls>' and end token '<eos>' were attached to the beginning and the end of each encoded sequence. Each encoded sequence was then input into ESM-MSA-1b, to get a local embedding with dimension L×768, in which L indicates the sequence length. The local embeddings of all RBD sequences were flattened and stacked as one matrix. PCA dimension reduction was conducted by the sklearn.decomposition. PCA.fit_transform function implemented in Scikit-learn 1.1.1[4], with default parameters. Phylogeny inference was conducted by IQ-TREE 2.2.565[5] under default settings, based on RBD domain sequence alignment. Tree visualization was supported by iTOL 6.9.1[6] (Fig. S11)

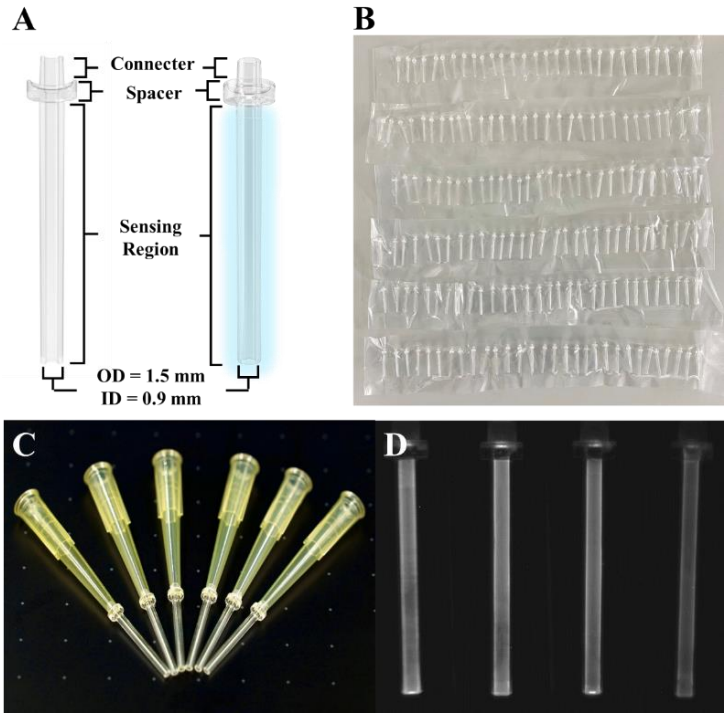

Figure S1. Microfluidic immuno-reactors used in the TOI system. (A) 3D structural illustration of a single TOI immuno-reactor. (B) TOI immuno-reactors fabricated through industrial-grade microscale injection molding, with a batch size of 10,000 and a defective rate < 0.1%. (C) TOI immuno-reactors connected to standard 200 μL pipette tips. (D) Chemiluminescent images of four TOI immuno-reactors.

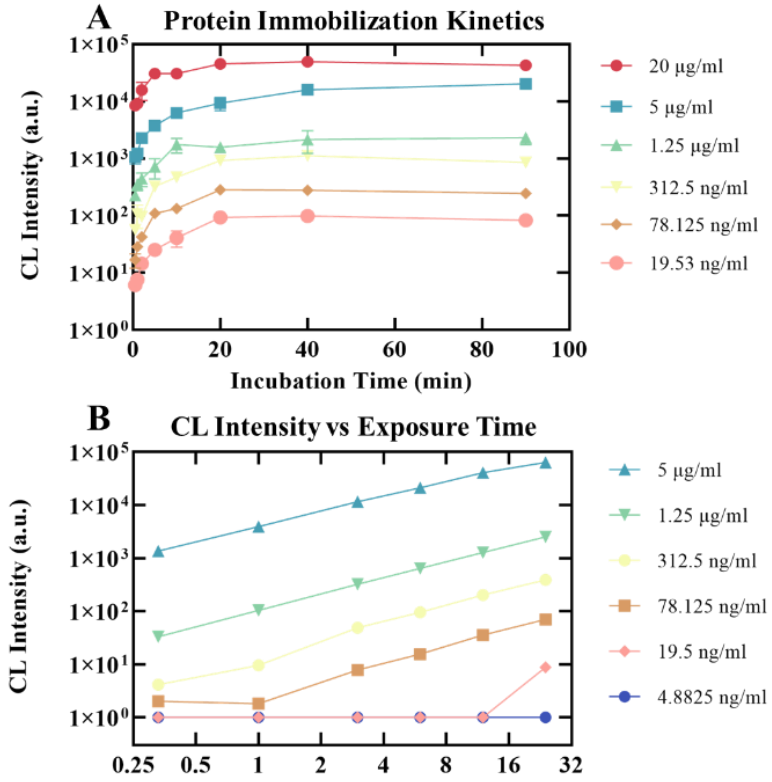

Figure S2. Performance evaluation of the TOI system. (A) The protein immobilization kinetics of the microfluidic immuno-reactors. For typical proteins such as IgG, the physical adsorption generally saturates after 20-40 minutes, significantly faster than conventional immunoassay reactors like 96-well plates. (B) Sensing performance of the luminol chemiluminescent signal detected through a QHY533M CMOS camera. Nonthermal noise was detected even with 12 seconds of exposure time (marked as 0.1), thanks to the high performance of the semiconductor cooling system in the camera. The minimum detectable optical signal intensity of the camera was 1.0, and the linear dynamic range was about 60,000 (gain = 70), covering 4.5-5 orders of magnitude in optical signal intensity.

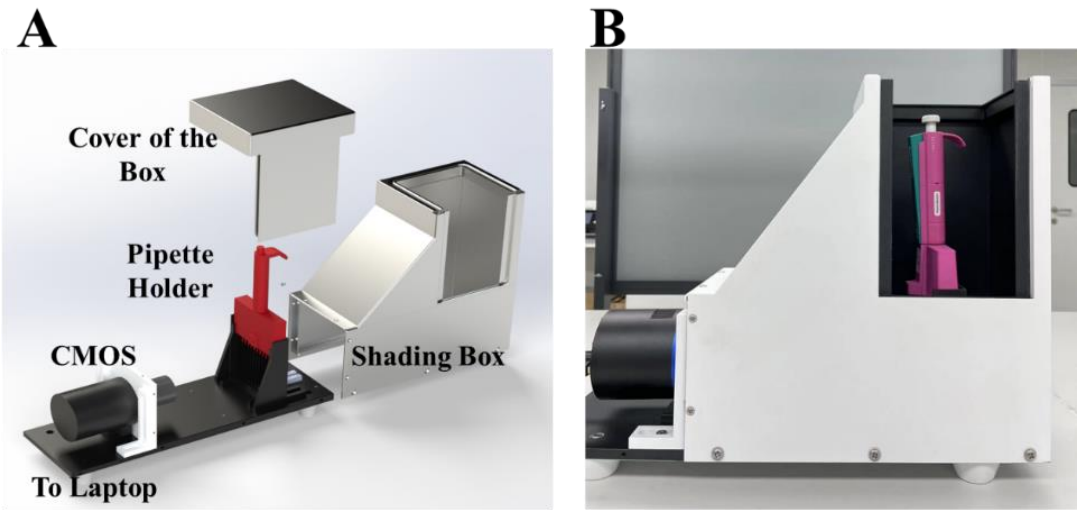

Figure S3. The TOI chemiluminescent imaging station. (A) 3D structural illustration of a TOI portable chemiluminescent imaging station (PCIS). (B) A side view photo (with the cover open) of the PCIS, including the shading cover, pipette holder, and CMOS camera of the PCIS.

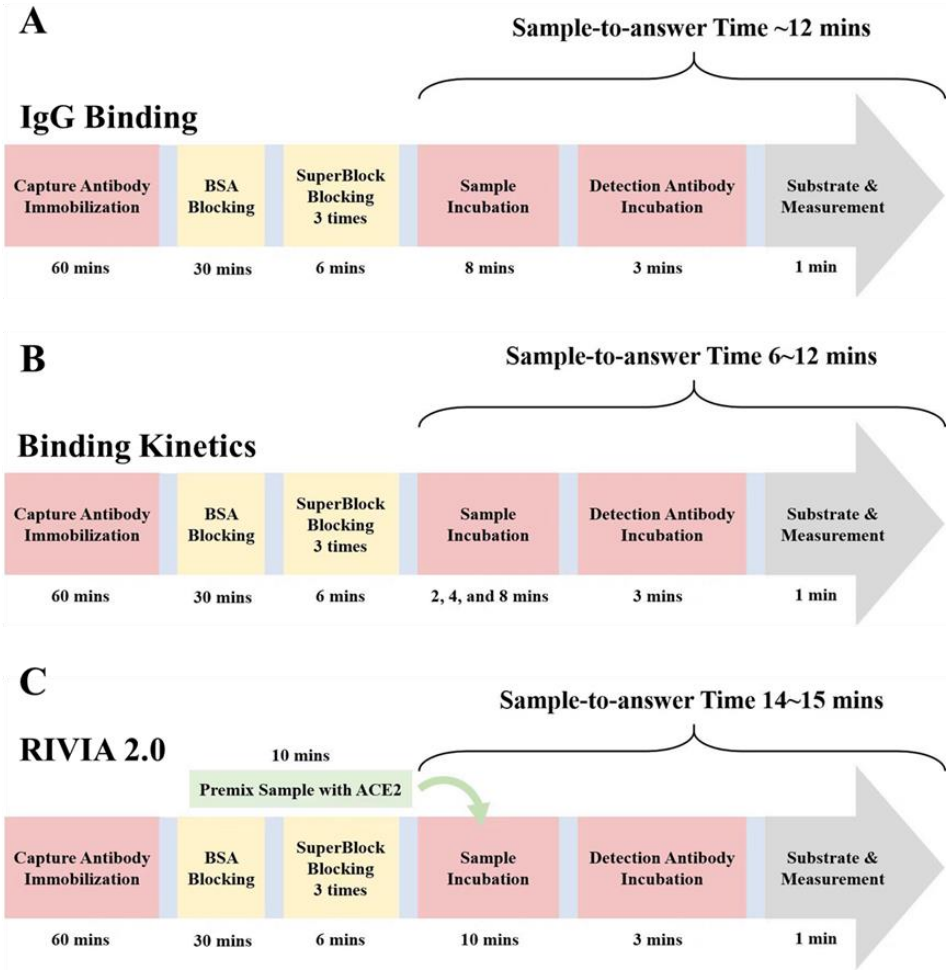

Figure S4. Graphical illustration of the experimental protocols used in TOI assays. (A) The protocol of the IgG binding assays used for the RBD monomer and the S-ECD trimer. The sample-to-answer time was approximately 12 minutes. (B) The protocol of the IgG binding kinetics assays for antibody affinity measurements. The sample-to-answer times were 6-12 minutes, depending on the incubation time. (C) The protocol of the rapid in-vitro inhibition assay (RIVIA 2.0). Diluted fingertip blood samples were pre-mixed with recombinant and engineered ACE2. The sample-to-answer time was approximately 15 minutes. For all assays, the light blue block after each incubation step indicates a quick rinsing with PBST.

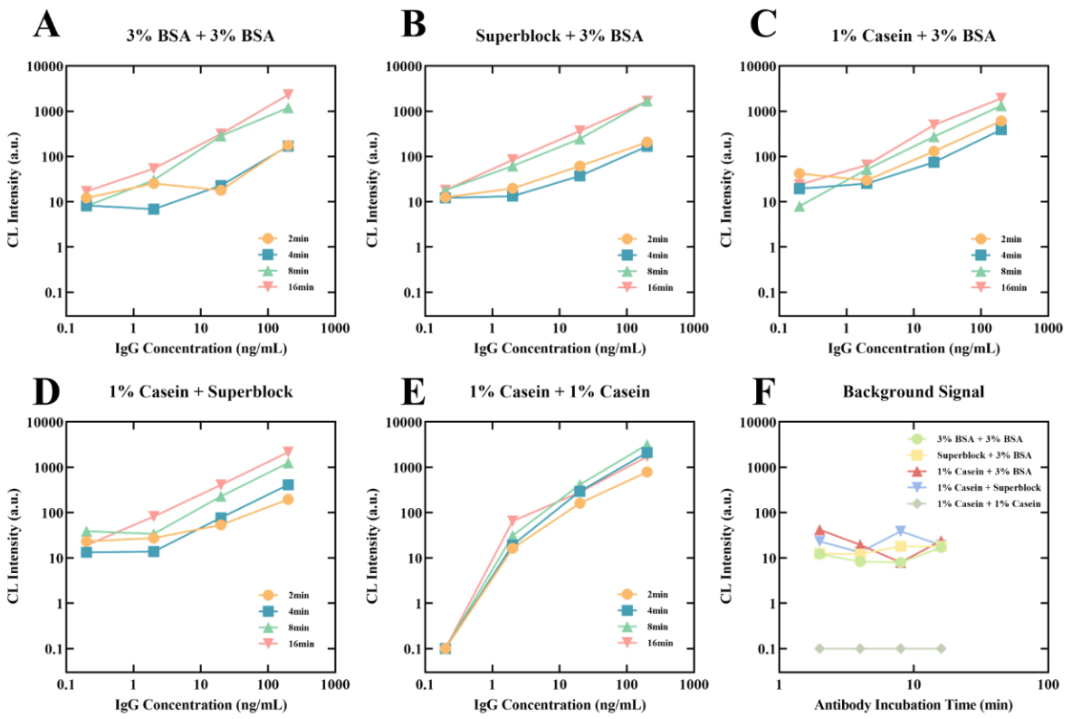

Figure S5. Optimization of the blocking buffer and the sample dilution buffer. All assays were conducted according to the protocol described in Figure S4, with SARS-CoV-2 WT RBD as the target antigen and SA55 antibody as the analyte. Various combinations of dilution buffers and incubation times were tested. 3% BSA in PBS, Superblock in PBS, and 1% Casein in PBS were the three major candidates for immunoassay dilution buffer.

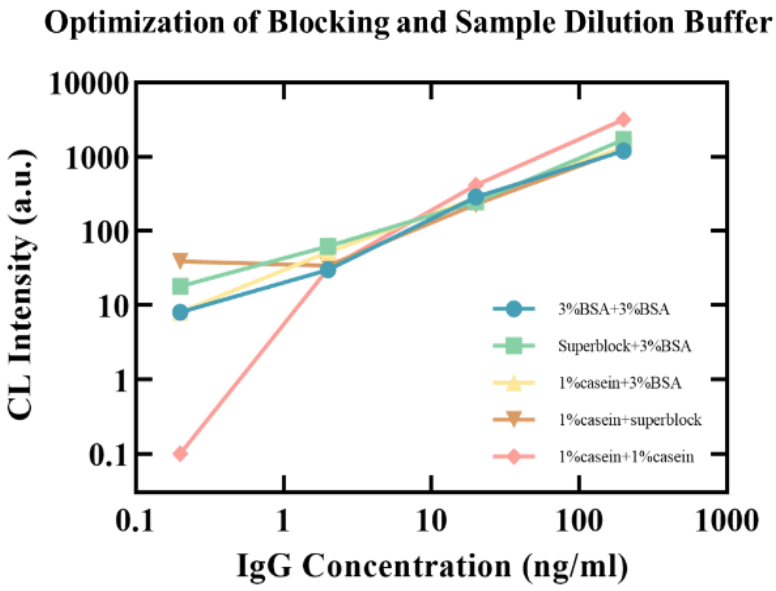

Figure S6. A summarized plot for buffer optimization. The background noise level decreased significantly (nearly zero, indicated as 0.1 on the plot) when using 1% casein in PBS for both immuno-reactor blocking and sample/reagent dilution.

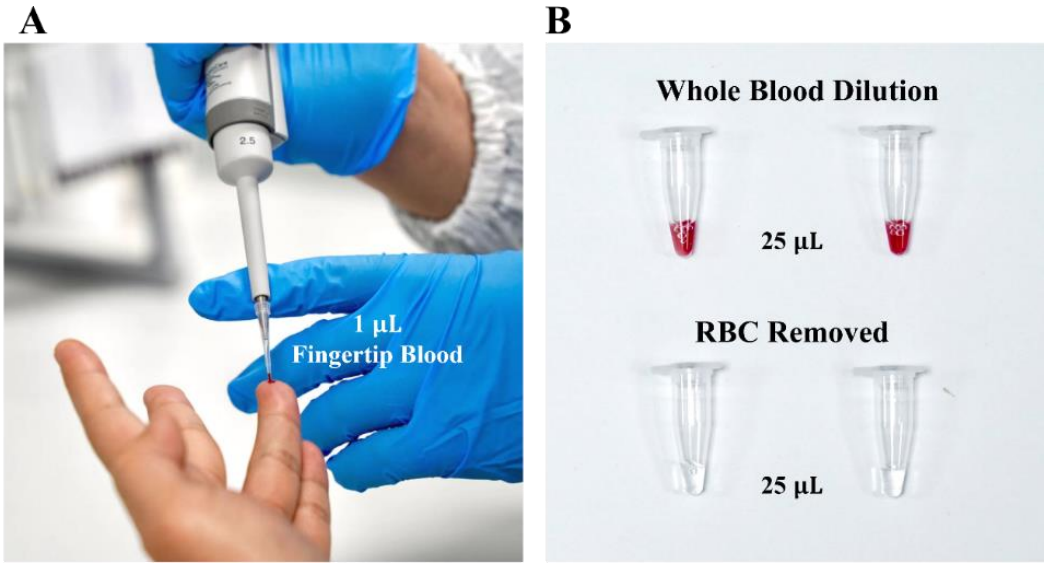

Figure S7. Photo records of the fingertip blood collection process for volunteers. (A) The collection process of 1 μL fingertip whole blood from a healthy volunteer. (B) Collection of the 25 × diluted fingertip blood samples and the RBC removal through quick centrifugation before storage.

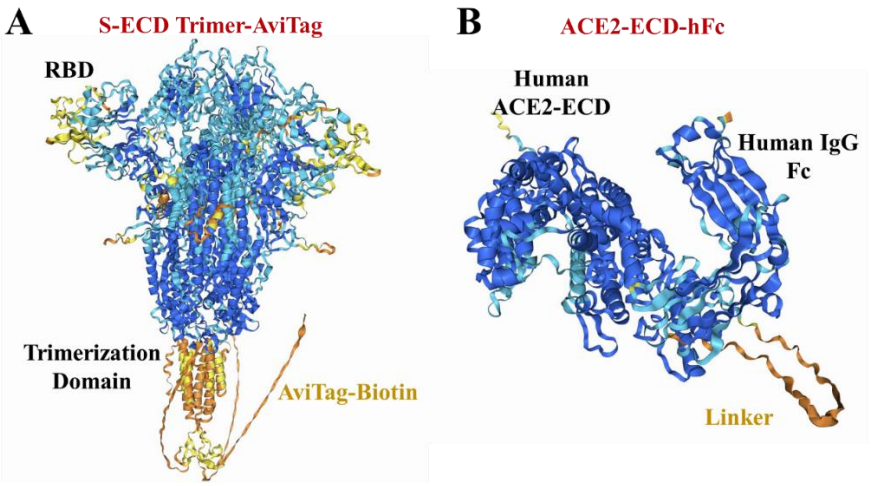

Figure S8. Alphafold3 simulations of the two designed protein probes used in RIVIA 2.0 generated with open-source Alphafold3. (A) The trimeric structure of S-ECD Trimer-AviTag. The T4 trimerization domain attaches to the N terminal of the S-ECD. His-tags and AviTag-biotins were all designed at the end of each sequence. (B) The Alphafold3 simulation of hACE2-ECD-hFc. The human IgG Fc domain is designed to connect with TOI immuno-reactors.

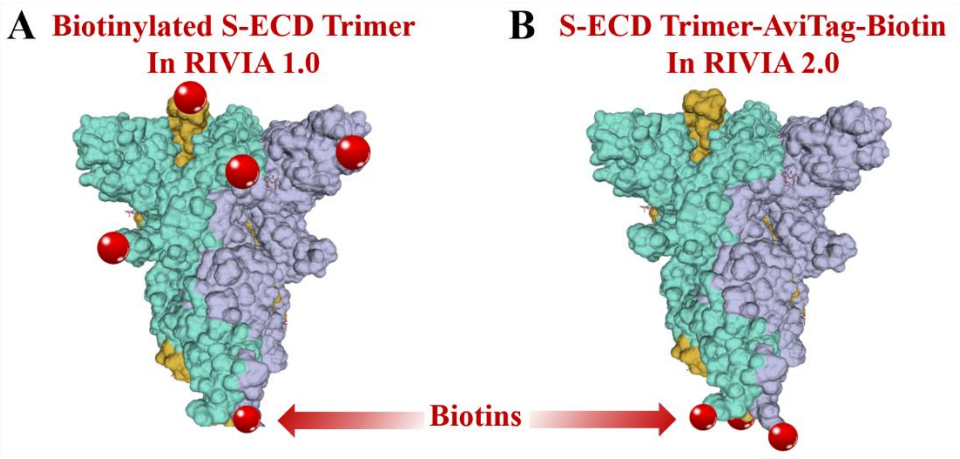

Figure S9. Simulations of the S-ECD trimers used in RIVIA 1.0 and 2.0., with the backbone generated using the Swiss model website. (A) For the S-ECD trimers used in RIVIA 1.0, biotins were chemically conjugated at random sites. The RBD binding epitopes may interfere during this conjugation process. (B) The engineered S-ECD Trimer-AviTag protein used in RIVIA 2.0., with three biotin reporters expressed at the N-terminal ends of the S-ECD monomer. The highly specific biotinylation sites were expected to have reduced interference with receptor binding.

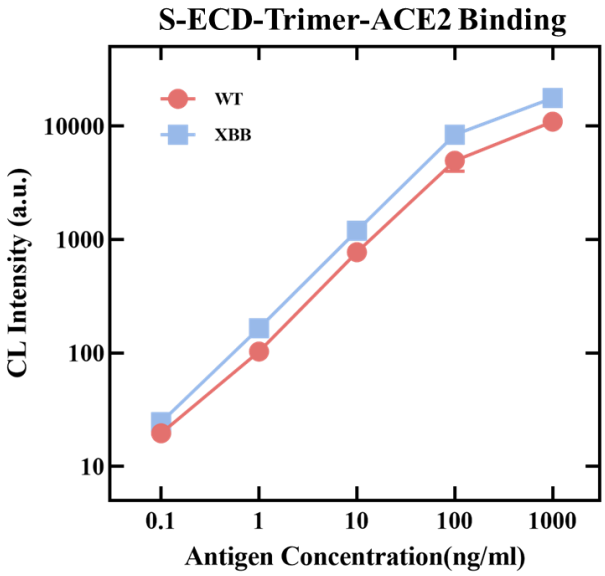

Figure S10. Binding curves generated with engineered S-ECD-Trimer-AviTag and recombinant ACE2-hFc. In all experiments, 15 μg/mL of ACE2-hFc were coated on immuno-reactors. S-ECD-Trimer constructed based on the XBB strain has a slightly stronger binding affinity compared with the S-ECD-Trimer of the WT strain.

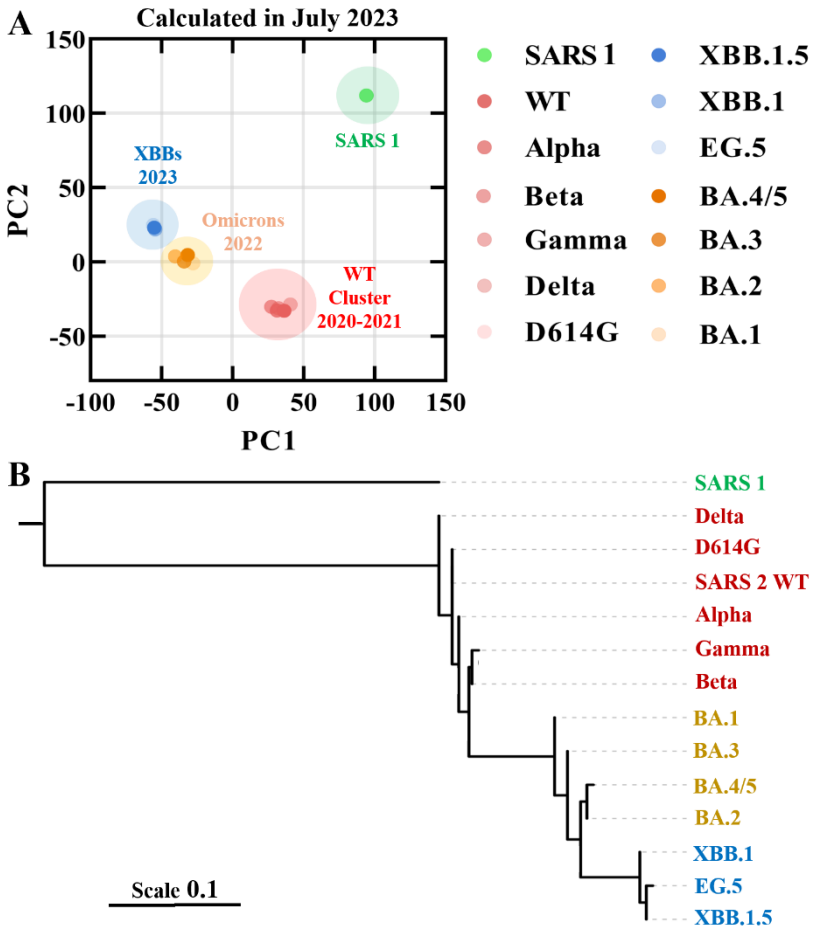

Figure S11. Antigenic map calculated using ESM-MSA-1b protein language model (A) and phylogenic tree (B) of different SARS-CoV variants based on published RBD sequences. The calculation was conducted in July 2023. The variants in the XBB family appear to have the farthest antigenic distance from the SARS CoV-2 WT strain reported in 2020. Thus, in our immune-response specificity evaluation experiments, WT and XBB (XBB1.16) were selected as model strains. Scale: mutation per amino acid.

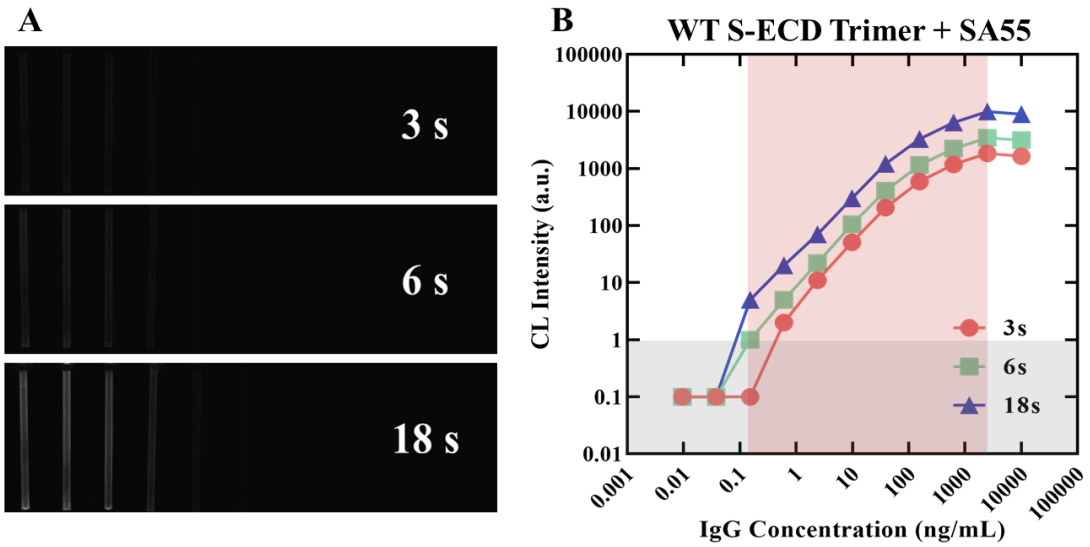

Figure S12. Visual demonstration of the IgG binding assay performance. All experiments were conducted with SARS-CoV-2 WT S-ECD trimer as the target antigen and SA55 antibody as the model analyte. (A) Chemiluminescent images collected at exposure times of 3s, 6s, and 18s respectively. (B) Quantification of the chemiluminescent signals from the images. An exposure time of 6s is enough for the generation of a measurable signal, even with only 0.1 ng/mL of SA55. The dynamic range of this IgG binding assay covers 0.1-3000 ng/mL (~4.5 orders of magnitude), and the weakest measurable signal intensity was 1.0 (above the grey-shaded area). Upon optimization, the signal-to-noise ratio for the IgG binding assays could reach >10000.

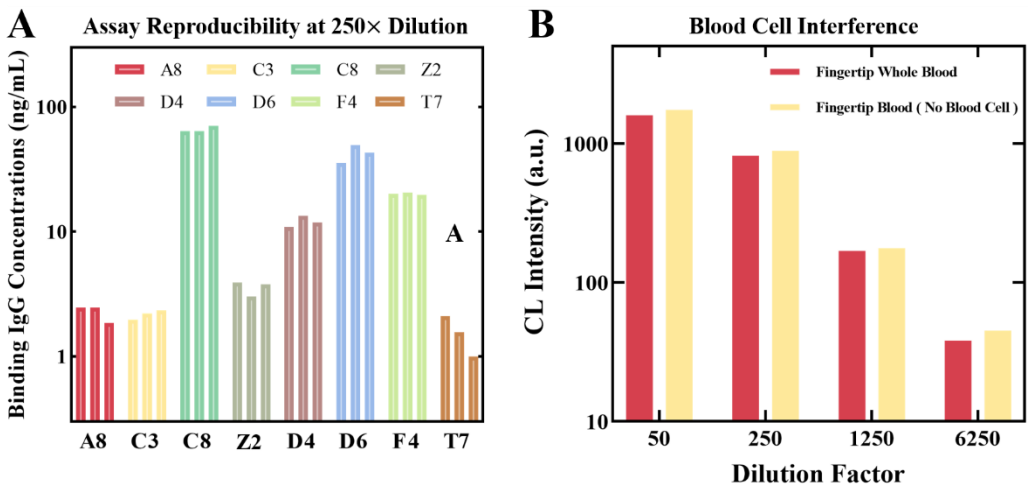

Figure S13. Reproducibility and robustness of fingertip blood-based immunoassays. (A) Triplicate measurements of typical IgG binding assays using SARS-CoV-2 WT RBD as the target antigen and 250 × diluted fingertip blood as the sample. The coefficient of variation (CV) for these assays ranged from 5% to 20%, suggesting that a single-point measurement is sufficient for quantitative IgG binding evaluation. (B) A comparison study of RBD binding antibody level measurements generated with a fingertip blood sample before and after removing the blood cells through centrifugation. The interference of blood cells is not significant in the IgG binding assays for samples diluted at 250 ×.

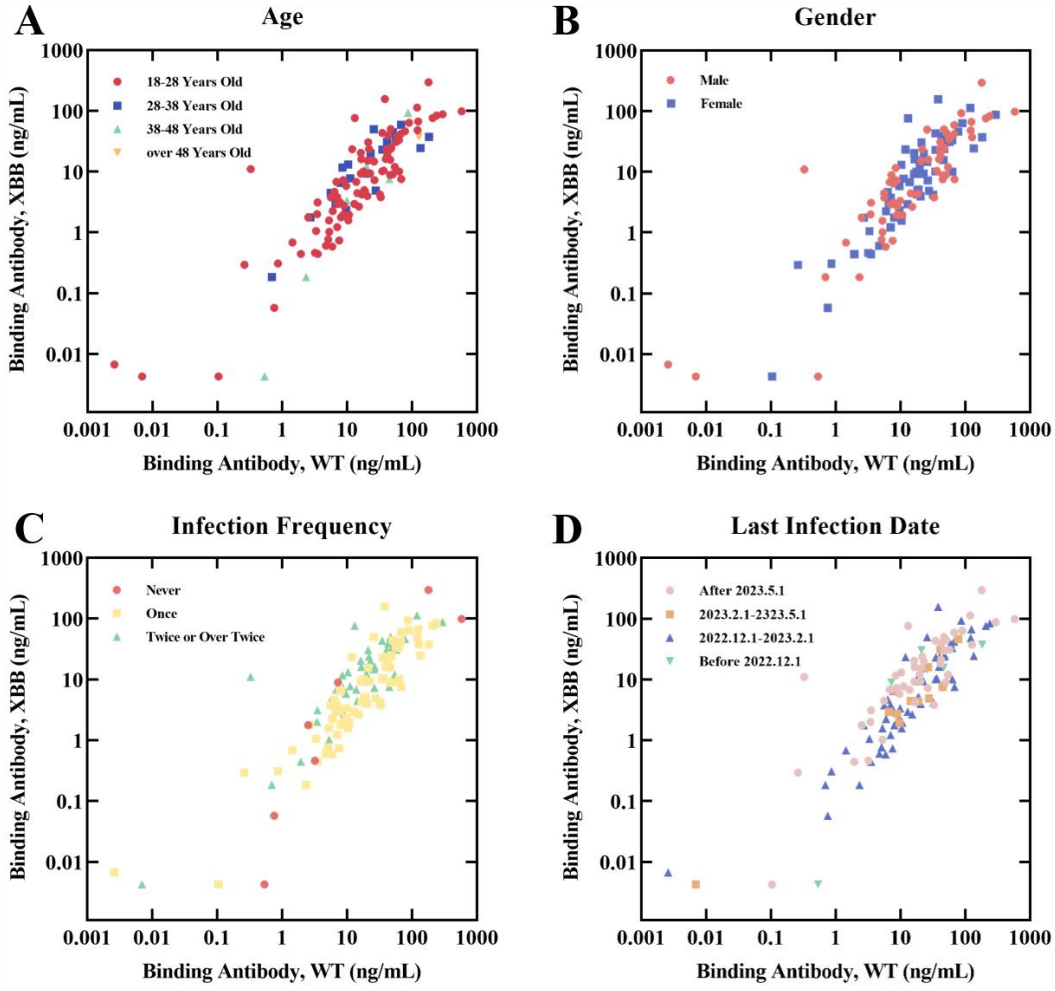

Figure S14. Raw data of the volunteers' binding IgG level against WT and XBB RBDs labeled with different classification methodologies. (A) Classification based on the age of volunteers at the time of sample collection. (B) Classification based on the gender of the volunteer; (C) Classification based on the infection frequency and (D) The last infection date.

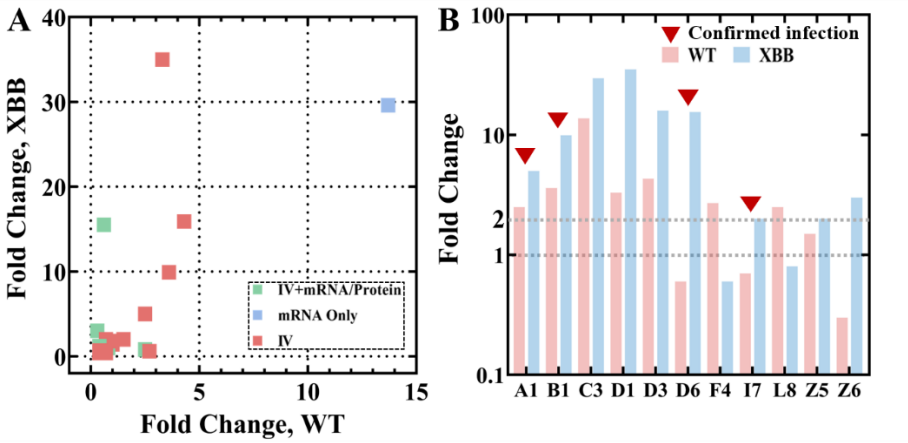

Figure S15. Fold changes in volunteers' WT and XBB antibody levels across a 6-month interval (Sep.2023-Mar.2024). (A) Linear-linear scale fold changes in WT and XBB IgG concentration of 22 volunteers displayed based on inoculation types. (B) The fold change for WT and XBB IgG concentration of 11 representatives from the longitudinal study, with the fold change of either type of antibody $\geqslant$ 2. Nine of them appeared to have a significant elevation in IgG level for XBB RBD, compared with that of the WT. Red triangle: confirmed SARS-CoV-2 infection between Sep.2023 and Mar.2024.

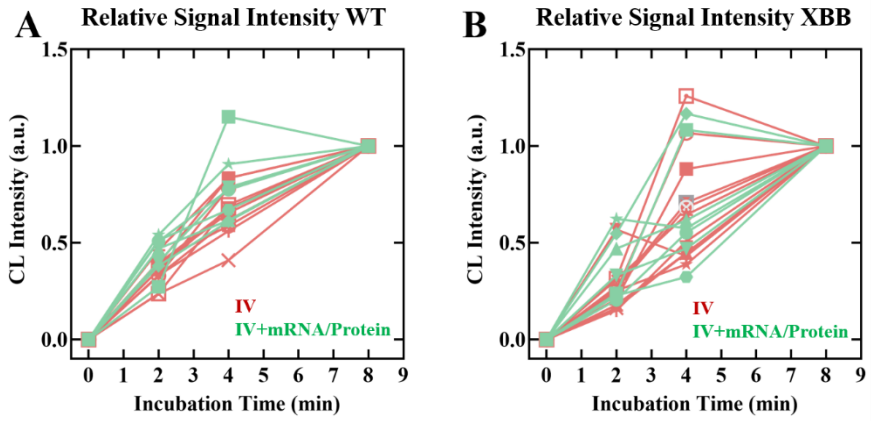

Figure S16. Relative signal intensities for the binding kinetics measurements. For the WT (A) and XBB variants (B), signals collected from 2 minutes and 4 minutes of incubation times were normalized to relative signal intensities, calculated by dividing the signal intensity with corresponding signal intensity of 8-minute incubation tests.

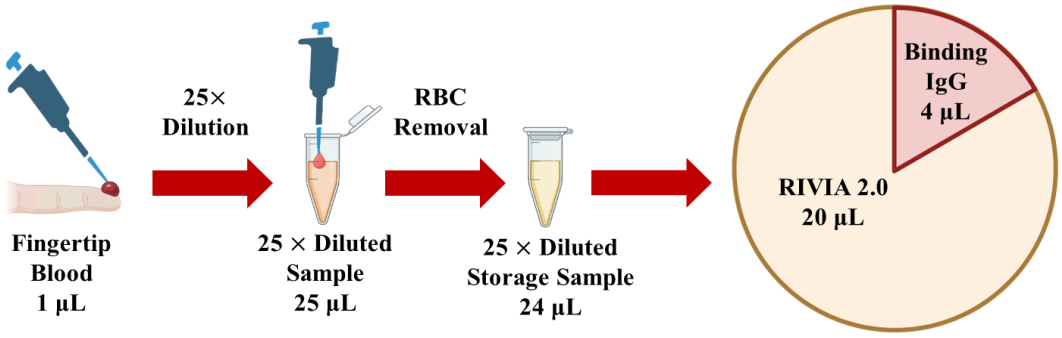

Figure S17. Sample usage of the 1 µL fingertip blood sample. 16.7% were consumed in RBD-binding IgG quantification assays (for two strains) and 83.3% were consumed in inhibition efficiency measurements.

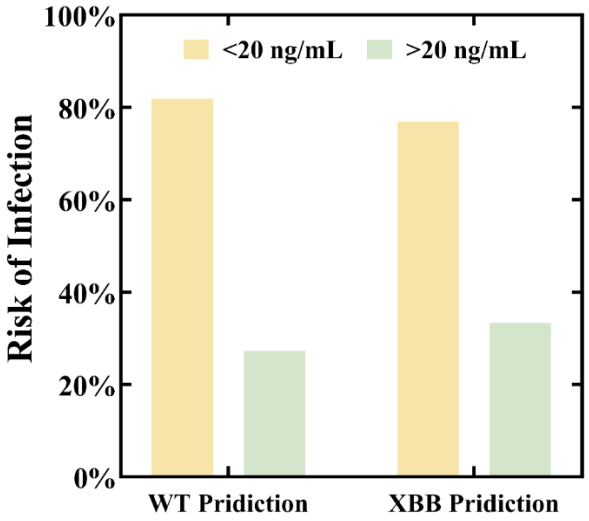

Figure S18. Infection risks assessment for the following six months (post-measurement) using effective binding IgG levels. When using 20 ng/mL of WT RBD binding IgG as the cutoff level (5 μL in the original serum, before dilution), the chance of SARS-CoV-2 re-infection within the following 6 months was 81.8% and 27.3% for the two groups, respectively. When using 20 ng/mL of XBB RBD binding IgG as the cutoff level, the chance of SARS-CoV-2 re-infection within the following 6 months was 76.9% and 33.3% for the two groups, respectively.

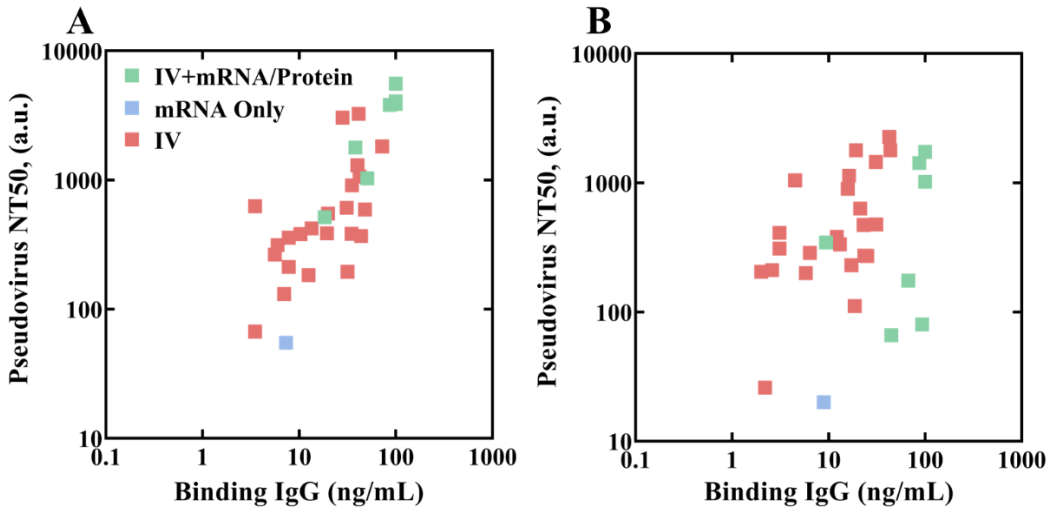

Figure S19. Scatter plots for binding IgG level against pseudovirus neutralization test for WT (A) and XBB (B). The binding IgG concentration and NC50 of WT demonstrate a better linear correlation compared with that of the XBB strain. RBD binding IgG at 20 ng/mL is roughly equivalent to IC50 = 300 for both strains.

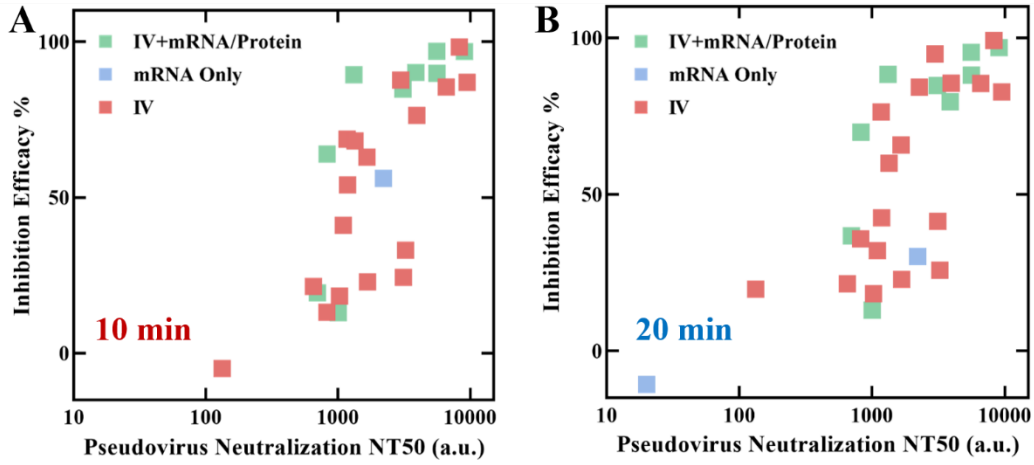

Figure S20. The dynamic range of RIVIA 2.0 can be slightly adjusted through the adjustment of sample incubation time. All results were generated with 50 × diluted fingertip blood and BA.4/5's S-ECD-Trimer. (A) Inhibition rates measured at 10 minutes of incubation time, where less signal saturations were observed. (B) Inhibition rates measured at 20 minutes of sample incubation time. More signal saturations were observed, especially for those samples with very high antibody levels. Such observations indicate that a longer sample incubation may be needed for measurements with low-abundance samples.

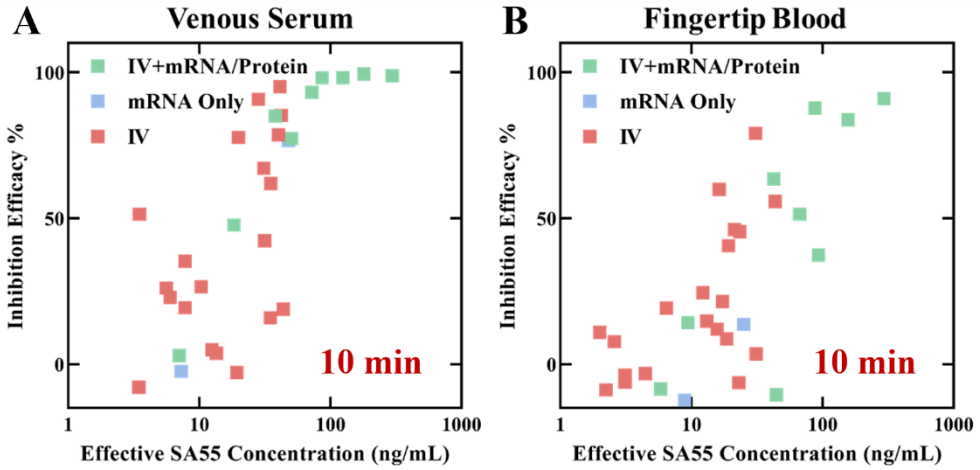

Figure S21 Differences between the RIVIA 2.0 results generated with venous serum samples and fingertip whole blood samples. All samples were diluted to 50 × using 1% casein, the target protein for both assays was XBB S-ECD-Trimer. (A) More signal saturations were observed for the sample with higher binding antibody levels. (B) Fewer signal saturations were observed for the sample with higher binding antibody levels. More samples fall out of the analyzable region (>30 inhibition rate). Such differences may be caused by the one-fold concentration difference of IgG between whole blood and serum (due to the volume of blood cells). Despite the differences, they still share a very similar trend.

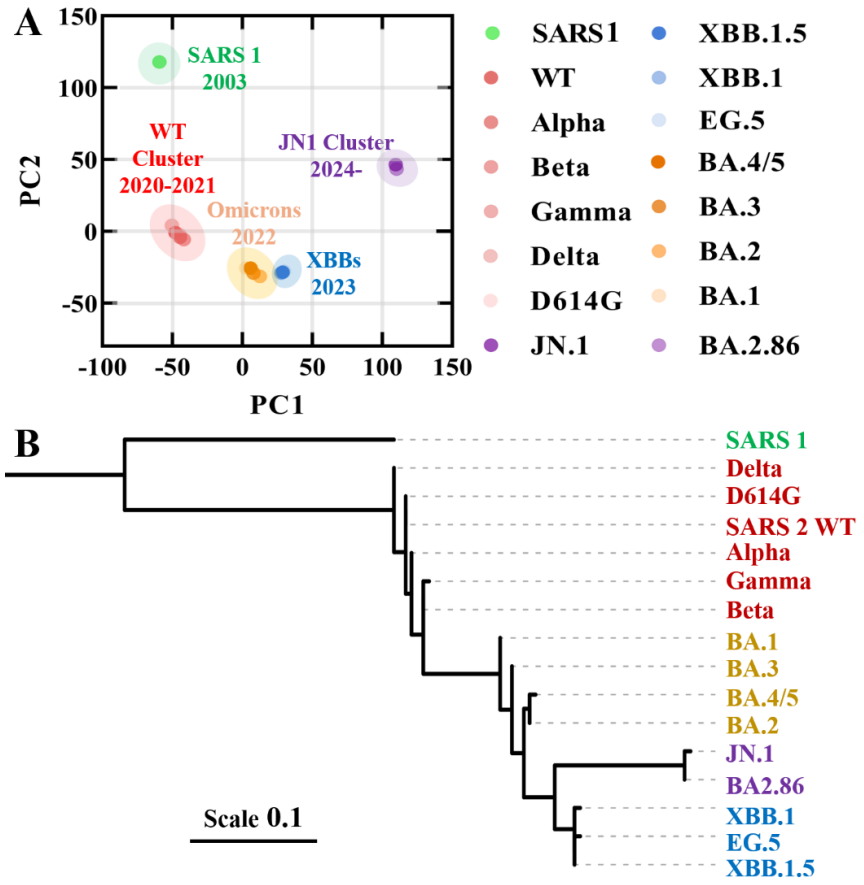

Figure S22. Antigenic map (A) and the phylogenic tree (B) for SARS-CoV RBD calculated in June 2024. JN1 (including but not limited to JN1, BA.2.86, KP.1, KP.2, and KP.3) cluster emerged during the years 2023 and 2024. By this time, XBB was no longer the variant that had the longest antigenic distance from the WT. The significant antigenic drift of SARS-CoV-2 variants could be observed almost annually, implying a strong immune pressure in the population. Scale: mutation per amino acid.

Table S1. Comparison of the conventional platforms with the TOI system.

Methodology	Time (hour)	Cost for two variants (USD)	Note
ELISA	2	80	Cost for an 8-point titration curve with plate-based ELISA
TOI-IgG Binding	0.2	5	Single-point quantitative measurement
SPR	1	1200	Kinetic measurement with specialized systems and chips
TOI-IgG Binding Kinetics	0.2	15	Three incubation time points per sample
VNT	72	600	Inhibition/Neutralization measurements with pseudovirus and live cells
TOI-RIVIA 2.0	0.3	30	A single point *in vitro* inhibition measurement with engineered proteins

Table S2. Fingertip blood test results of the IgG binding assay for WT and XBB strain using the TOI system (sampled in September 2023, n = 113). The unit of test results is chemiluminescent intensity.

ID	WT	XBB	ID	WT	XBB	ID	WT	XBB
A1	16.8	4.2	E7	7.5	0.7	J5	57.4	30.9
A2	14.4	4.4	E8	0.9	0.3	J6	18.6	4.4
A3	8	1.8	F1	17.8	10.1	J7	67.7	59
A4	10.4	1.6	F2	9.7	5.8	J8	26.1	14.7
A5	47.3	23.8	F3	10.7	1.9	K1	90.1	63.7
A6	0.1	0.1	F4	13.2	76.2	K2	78.1	46.3
A7	36.4	10.4	F5	19.2	5.1	K3	21.8	23.7
A8	2.7	1.8	F6	26.9	15.9	K4	16.5	16
B1	9.7	2.3	F7	6.8	6.8	K5	22.7	9.3
B2	21.1	30.3	F8	9	2.7	K6	18.5	5
B3	122	48.2	G1	7.1	3.8	K7	6.4	4.7
B4	41.5	18.3	G2	0.7	0.2	K8	46.9	50.1
B5	20.5	4	G3	8.7	1.9	L1	20.8	15.2
B6	5.9	0.6	G4	1.9	0.4	L2	0.1	0.1
B7	7.1	2.9	G5	3.3	1.1	L3	16.3	20.3
B8	23	19.8	G6	2.5	1.8	L4	11.9	23.5
C1	182.3	37.5	G7	12.9	2.9	L5	62.9	33
C2	126.9	37.5	G8	8.5	11.7	L6	8.1	6.6
C3	0.5	0.1	H1	16.2	9.3	L7	67.1	41.9
C4	3.5	0.4	H2	0.1	0.1	L8	119.6	112.8
C5	32	4.2	H3	46.2	15.6	M1	13.5	15.8
C6	26.3	7.3	H4	3.2	0.5	M2	19.4	19.2
C7	68.5	7.5	H5	1.4	0.7	M3	31.6	18.7
C8	207.4	76.2	H6	4.7	0.6	M4	28.2	16.3
D1	2.3	0.2	H7	13.8	6.8	M5	7	5.8
D2	27.7	4.9	H8	0.3	11	M6	31.1	17.2
D3	9.7	1.9	I1	34.9	10.1	M7	12.5	2.6
D4	11.1	7.8	I2	5.6	3.7	M8	43.7	31.2
D5	135.5	24.5	I3	0.8	0.1	N1	72.3	42.5
D6	63.3	10.1	I4	5.1	0.8	Y1	56.6	34.7
D7	44.8	7.5	I5	21.2	15.5	Y2	25.8	49.6
D8	32.9	3.8	I6	15.2	2.7	Z1	39.4	16.2
E1	54.4	12	I7	5.3	1	Z2	8.7	7.3
E2	20.2	9.3	I8	50.2	9	Z3	239.2	83.5
E3	6.6	2.9	J1	45.7	8.9	Z4	47.3	30
E4	7.1	1.2	J2	0.3	0.3	Z5	5.3	1.6
E5	9.9	3.3	J3	43.2	39.2	Z6	582.9	98.1
E6	0.1	0.1	J4	60.2	38.2			

Table S3. Longitude IgG binding test data for WT and XBB strain using TOI system. The fingertip blood samples of 22 individuals were collected in September 2023 and March 2024. The unit of test results is chemiluminescent intensity.

Strain	**WT**		**XBB**	
Sampling time	2023.09	2024.03	2023.09	2024.03
A1*	16.8	42.3	4.2	21.3
B1*	9.7	35.2	2.3	23.1
B3#	122	48	48.2	25.1
B8#	23	10.3	19.8	13.1
C3*	0.5	7.3	0.1	8.9
C8	207.4	86.7	76.2	93.3
D1*	2.3	7.8	0.2	6.4
D3*	9.7	41.3	1.9	30.9
D6*	63.3	38.1	10.1	156.7
E4	7.1	6	1.2	2.2
F4*	13.2	34.9	76.2	43.5
G8#	8.5	5.6	11.7	4.5
I7*	5.3	3.5	1	2
J7#	67.7	50.8	59	44.6
K5	22.7	18.4	9.3	9.4
L8*	119.6	296.7	112.8	87.4
Z1	39.4	40.2	16.2	23.4
Z2#	8.7	3.5	7.3	3.1
Z3#	239.2	124.9	83.5	66.9
Z4#	47.3	19.9	30	12.2
Z5*	5.3	7.8	1.6	3.2
Z6*	582.9	180.3	98.1	294.9

Note: #: signals of both WT and XBB IgG binding tests decreased; *: at least one of the signal fold change $\geqslant 2$.

Table S4. Test result of IgG binding assay, RIVIA 2.0, and pVNT for 31 volunteers. Assays conducted with the TOI system (B and R) were performed with fingertip blood, while the pVNTs (P) were performed with venous serum.

Strain	**WT**			**XBB**		
Assays ID	IgG Binding (B)	RIVIA 2.0 (R)	pVNT (P)	IgG Binding (B)	RIVIA 2.0 (R)	pVNT (P)
A1-2	42.3	85.2	1061	21.3	46.2	631
B1-2	35.2	61.9	908	23.1	0	471
B3-2	48	76.7	591	25.1	0	271
B8-2	10.3	26.5	382	13.1	14.7	334
C3-2	7.3	0	55	8.9	0	20
C8-2	86.7	98.1	3808	93.3	37.3	80
D1-2	7.8	19.3	357	6.4	19.2	287
D3-2	41.3	95.1	3249	30.9	79.1	1449
D6-2	38.1	85	1783	100	83.7	1018
E4-2	6	22.9	313	2.2	0	26
F4-2	34.9	15.9	383	43.5	55.8	1783
G8-2	5.6	26.1	264	4.5	0	1045
I7-2	3.5	0	67	2	10.9	205
J7-2	50.8	77.3	1030	44.6	0	66
K5-2	18.4	47.7	515	9.4	14.3	345
L8-2	100	98.8	4061	87.4	87.8	1421
M1	13.5	0	420	15.8	12	897
M2	19.4	0	386	19.2	40.6	1785
M3	31.6	42.3	195	18.7	8.6	111
M4	28.2	90.7	3041	16.3	59.9	1133
M5	7	2.9	131	5.8	0	200
M6	31.1	67.1	609	17.2	21.4	230
M7	12.5	4.9	183	2.6	7.7	211
M8	43.7	18.8	368	31.2	3.5	475
N1	72.3	93.1	1817	42.5	63.5	2262
Z1-2	40.2	78.6	1296	23.4	45.4	273
Z2-2	3.5	51.3	626	3.1	0	309
Z3-2	100	98.2	3867	66.9	51.3	175
Z4-2	19.9	77.7	550	12.2	24.5	381
Z5-2	7.8	35.3	212	3.1	0	410
Z6-2	100	99.5	5571	100	91	1731

Note: ID with -2 indicates the sample was collected in March 2024, otherwise the sample was collected in September 2023. pVNT: pseudovirus neutralization test.